PNAS RESEARCH ARTICLE | ENGINEERING OPEN ACCESS

Mechanical ventilation energy analysis: Recruitment focuses injurious power in the ventilated lung

Donald P. Gaver III[a,1], Michaela Kollisch-Singule[b], Gary Nieman[b], Joshua Satalin[b], Nader Habashi[c], and Jason H. T. Bates[d]

Affiliations are included on p. 11.

Edited by Howard Stone, Princeton University, Princeton, NJ; received September 26, 2024; accepted January 22, 2025

The progression of acute respiratory distress syndrome (ARDS) from its onset due to disease or trauma to either recovery or death is poorly understood. Currently, there are no generally accepted treatments aside from supportive care using mechanical ventilation. However, this can lead to ventilator-induced lung injury (VILI), which contributes to a 30 to 40% mortality rate. In this study, we develop and demonstrate a technique to quantify forms of energy transport and dissipation during mechanical ventilation to directly evaluate their relationship to VILI. A porcine ARDS model was used, with ventilation parameters independently controlling lung overdistension and alveolar/airway recruitment/derecruitment (RD). Hourly measurements of airflow, tracheal and esophageal pressures, respiratory system impedance, and oxygen transport were taken for six hours following lung injury to track energy transfer and lung function. The final degree of injury was assessed histologically. Total and dissipated energies were quantified from lung pressure–volume relationships and subdivided into contributions from airflow, tissue viscoelasticity, and RD. Only RD correlated with physiologic recovery. Despite accounting for a very small fraction (2 to 5%) of the total energy dissipation, RD is damaging because it occurs quickly over a very small area. We estimate power intensity of RD energy dissipation to be 100 W/m^2, equivalent to 10% of the Sun's luminance at the Earth's surface. Minimizing repetitive RD events may thus be crucial for mitigating VILI.

ARDS | ventilator-induced lung injury | energy dissipation | power

Significance

Acute respiratory distress syndrome (ARDS) is a commonly fatal condition that is managed with mechanical ventilation, which can unfortunately lead to ventilator-induced lung injury (VILI). This study explores how forms of energy delivery/dissipation from mechanical ventilation are linked to biomarkers of VILI. Herein, we present a robust technique to identify energy delivery/dissipation due to airflow, tissue deformation, and alveolar/airway recruitment. Both tissue deformation and recruitment have been hypothesized to contribute to VILI. This study provides a quantitative method to evaluate those hypotheses and identifies recruitment as being far more injurious despite its far smaller magnitude. This study provides an avenue for patient-centered treatment that might reduce ARDS mortality.

Acute respiratory distress syndrome (ARDS) presents a global health challenge, as indicated by an international study that estimated that 10% of ICU admissions experienced ARDS (1). While supportive care using mechanical ventilation provides crucial treatment (2), it carries the risk of causing ventilator-induced lung injury (VILI) (3). Decades of research have been devoted to the reduction of VILI, spurred by the NIH ARDSnet study of the 1990's and beyond (4), leading to low-tidal volume ventilation as the standard of care for ARDS. Despite more than two decades of low-tidal volume ventilation, this approach still results in ARDS mortality rates that are unacceptably high at 30 to 40% (1, 5). There is thus a dire need for alternative approaches to mechanical ventilation that take individual patient pathophysiology into account. However, this requires greater precision in understanding the underlying mechanisms by which mechanical ventilation damages the lung.

It is well recognized that biomechanical insult contributes to VILI, with the focus on two mechanisms: 1) volutrauma (overdistension) and/or 2) atelectrauma (alveolar recruitment/derecruitment). It has been theorized that VILI can be linked to the energy delivered to, or dissipated within, the lungs from positive-pressure mechanical ventilation (6–12). While this notion is intuitively plausible given that any type of mechanical injury involves energy transfer, the specific types of energy transfer that cause lung damage remain unclear. Furthermore, the specific mechanisms underlying VILI are not immediately apparent from current surrogates of lung mechanics (e.g., tidal volume and plateau pressure). In this study, we invoke the energy transfer hypothesis to develop robust detection methods and identify markers associated with the cause of VILI.

During the ventilation cycle, energy is transferred to the lung in two forms: recoverable and dissipated. The recoverable form is returned to the environment in its entirety upon expiration, likely leaving no lasting impact on tissue structure. Recoverable energy might temporarily change the state of the tissue in a way that could facilitate injury propagation, such as by expanding elastic pores to allow transudation of plasma fluid into the air spaces, but this would not constitute tissue damage per se. Nevertheless, recoverable energy could temporarily change the state of the system in a manner that could propagate injury, so it is worth investigating.

Author contributions: D.P.G., M.K.-S., G.N., J.S., N.H., and J.H.T.B. designed research; D.P.G, M.K.-S., J.S., and J.H.T.B. performed research; D.P.G., M.K.-S., G.N., and J.H.T.B. analyzed data; and D.P.G., M.K.-S., G.N., N.H., and J.H.T.B. wrote the paper.

Competing interest statement: J.H.T.B. is a consultant and shareholder of OscillaVent, Inc. and Respiratory Sciences, Inc., and is consultant to Chiesi, Inc. M.K.-S. has received an educational research Grant from and has lectured for Dräger Medical Systems, Inc.

This article is a PNAS Direct Submission.

[1]To whom correspondence may be addressed. Email: dpg@tulane.edu.

This article contains supporting information online at https://www.pnas.org/lookup/suppl/doi:10.1073/pnas.2419374122/-/DCSupplemental.

Published March 3, 2025.

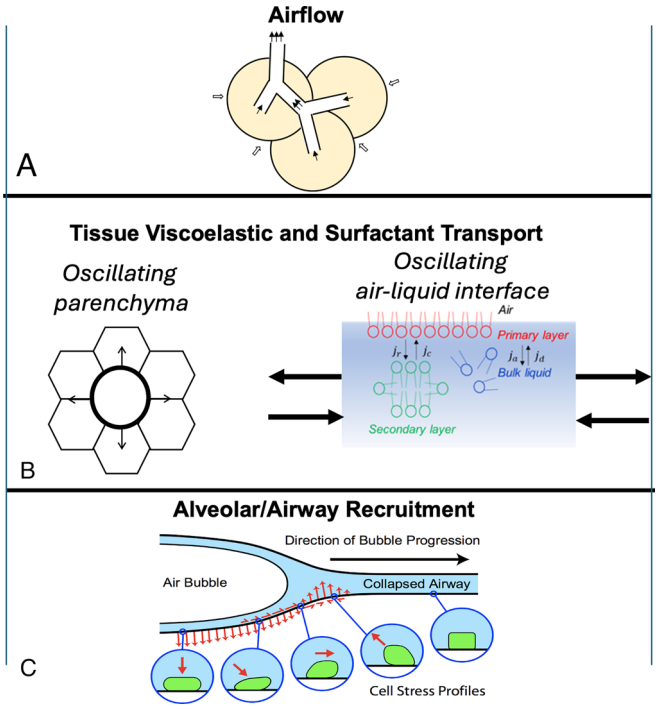

Fig. 1. Components of energy dissipation. (*A*) Airflow. (*B*) Tissue stretching and air–liquid interfacial deformation, including surfactant transport. (*C*) Recruitment of airways and alveoli, where energy is dissipated through viscous interactions as airway walls peel apart to overcome adhesive surface tension forces that hold walls in apposition.

By contrast, tissue damage is fundamentally irreversible and constitutes a dissipative process (12). Energy dissipation in the lung can arise from several different processes as shown in Fig. 1:

A. **Airflow resistance**: Energy is dissipated as air flows between the mouth and alveoli. Bronchoconstriction due to smooth muscle contraction and airway wall thickening increases the pressure drop required for breathing by creating greater resistance to airflow, making it more difficult to move air in and out of the lungs. This is a hallmark of asthma (13).
B. **Tissue-level viscoelastic responses**: Energy is dissipated as alveoli stretch to accommodate volume changes during tidal breathing. Normal surfactant transport within the lining fluid that coats the interior surfaces of airways and alveoli creates dynamic surface tension that stabilizes the lung (14). Pathologically, lung compliance is increased in emphysema and increases the work required to exhale. Conversely, surfactant deficiency and fibrosis decrease compliance and make lungs stiffer. This and increases the effort needed to inhale (15, 16).
C. **Airway/alveolar recruitment**: This occurs when airflow and parenchymal tethering work together to unblock lining fluid obstructions within airways and alveoli (17, 18). This process creates crackling sounds ("rales") that can be heard during inspiration through a stethoscope (19, 20).

Not all energy dissipation in the lung is injurious. Indeed, energy dissipation is an inherent feature of respiration. Airflow resistance primarily dissipates energy within the gas phase, minimizing direct tissue injury. Tissue viscoelasticity contributes to energy dissipation during normal breathing as an inescapable consequence of tissue structure. Dynamic surface tension contributes to energy dissipation at the air–liquid interface. However, tissue overdistension can be damaging, potentially evident by altered viscoelastic responses. Furthermore, dissipation due to the recruitment of collapsed air spaces, while not significant in healthy lungs during mechanical ventilation, becomes more prevalent and significant in injured lungs because the microstresses can be highly damaging to the epithelial tissue. While surfactants play a role in both tissue-level and recruitment dissipation, their effects differ, as detailed in *SI Appendix*.

Separating the normal components of energy dissipation from those that are abnormal and potentially injurious is thus an important clinical problem. To address this problem, we have developed methods to evaluate energy delivery and dissipation in a mechanically ventilated porcine model of ARDS in which lung tissue overdistention (OD) and cyclic intratidal recruitment and derecruitment (RD) were controlled independently of each other. Quantitative comparisons between physiological response and energetics allow us to determine which sources of energy dissipation had the most significance for VILI.

Experimental Overview. Our experiments involved the application of engineered ventilation waveforms using airway pressure release ventilation (APRV), with physiological responses and energy delivery dissipation monitored as follows:

Ventilation Protocols: Following injury, the animals were randomly divided into four groups OD+RD+, OD+RD–, OD–RD+, and OD–RD– according to whether they were subjected to or protected from overdistention (OD+ and OD–, respectively), and for recruitment and derecruitment (RD+ and RD–, respectively).

Physiological responses were tracked by

- **Oxygenation**, evaluated using the PaO_2/FiO_2 ratio, serves as a key indicator of physiologic respiratory health. This ratio quantifies oxygen transfer in the lungs and is calculated by dividing the partial pressure of oxygen in arterial blood (PaO_2, measured in mmHg) by the fraction of inspired oxygen (FiO_2). A lower PaO_2/FiO_2 ratio indicates impaired oxygenation, commonly observed in conditions such as ARDS, pneumonia, or hypoxemic respiratory failure, and is used to guide ventilator settings. A PaO_2/FiO_2 ratio below 300 mmHg is a diagnostic criterion for ARDS (21).
- **Respiratory mechanics**, assessed using a custom oscillometry setup (22) quantifies the biomechanical state of the respiratory tissues through the respiratory system compliance (C_{RS}—inverse of elastance). C_{RS} is defined as the change in lung volume per unit change in transpulmonary pressure and serves as an essential measure of lung elasticity and mechanical function. Clinically, reduced C_{RS} is a hallmark of restrictive lung diseases, including ARDS and pulmonary fibrosis, and indicates stiff or noncompliant lungs that is used to guide ventilator management. Thus, C_{RS} is both a diagnostic and prognostic tool used to optimize respiratory support in patients with compromised lung function. C_{RS} was normalized to each animal's value immediately following injury (nC_{RS}).
- **Histology**, using postmortem tissue sections from the right diaphragmatic lobe (Tween-injured tissue).

Energy delivery and dissipation measurements focused on the subcomponents depicted in Fig. 1 and their associated clinical observations:

- Airflow resistance (23),
- Tissue-level viscoelastic responses (16, 24, 25) associated with volutrauma (26), and
- Recruitment, associated with atelectrauma (18, 27–33).

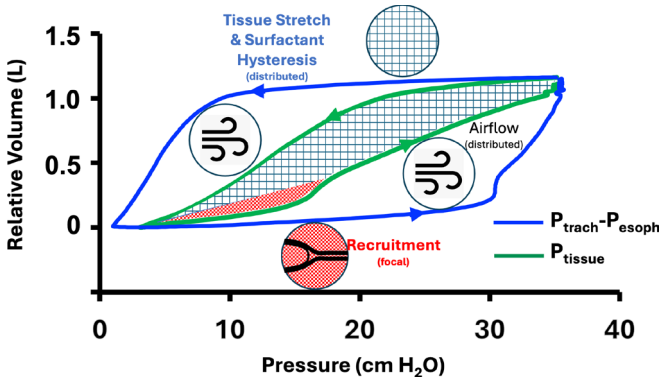

Fig. 2. Schematic of a pressure–volume loop, with P_{tp} in blue outline and the tissue pressure P_{tissue} in green outline. The subareas of these loops quantify the energy dissipation from airflow ($D_{airflow}$ = white), tissue level (D_{tissue} = blue hashed), and recruitment ($D_{recruit}$ = red hashed).

Fundamentally, energy delivered and dissipated within the lungs is determined by the dynamic relationship between transpulmonary pressure, $P_{tp}(t)$, and lung volume, $V(t)$, creating a PV hysteresis loop, whose area is the total dissipated energy. The energy delivered (input work) is the integral of $P_{trach}(t) * V(t)$ during the inflation phase.

The custom oscillometry approach allows the determination of dynamic alveolar-level pressures during breathing (P_{tissue}). The dissipation subcomponents ($D_{airflow}$, D_{tissue}, and $D_{recruit}$) are shown schematically in hysteresis loops in Fig. 2, with the calculations describing their magnitudes provided in the *Materials and Methods* and *SI Appendix*.

Results

Physiological Response. Fig. 3 illustrates the physiological responses under various ventilation scenarios. Injury was induced at time T0. We monitored pulmonary mechanics, specifically normalized respiratory system compliance (nC_{RS}), and oxygenation (PaO_2/FiO_2) over the next 6 h. This allowed us to assess the progression of the injury.

Fig. 3*A* demonstrates a postinjury increase in nC_{RS} at T1 for all animal groups, but this increase continues only for the two RD− groups. Treatment-based analysis (Fig. 3*B*) demonstrates statistical significance between RD+ and RD− groups, with nC_{RS} significantly greater for the two RD− scenarios, and no significant influence by either the presence or absence of OD. Fig. 3*B* data points represent time-point means from Fig. 3*A*, with error bars representing treatment mean ± SEM.

Fig. 3 *C* and *D* presents corresponding plots of oxygenation (PaO_2/FiO_2) as a clinically relevant quantitative biomarker of lung injury, with PaO_2/FiO_2 < 300 mmHg indicating ARDS (21). Immediately after injury at T0, all animals demonstrated PaO_2/FiO_2 ratios that were clinically significant for ARDS. Animals with neither OD nor RD (OD−RD−) demonstrated a rapid improvement in oxygenation whereas animals with both OD and RD (OD+RD+) had sustained lung injury (note that these are data

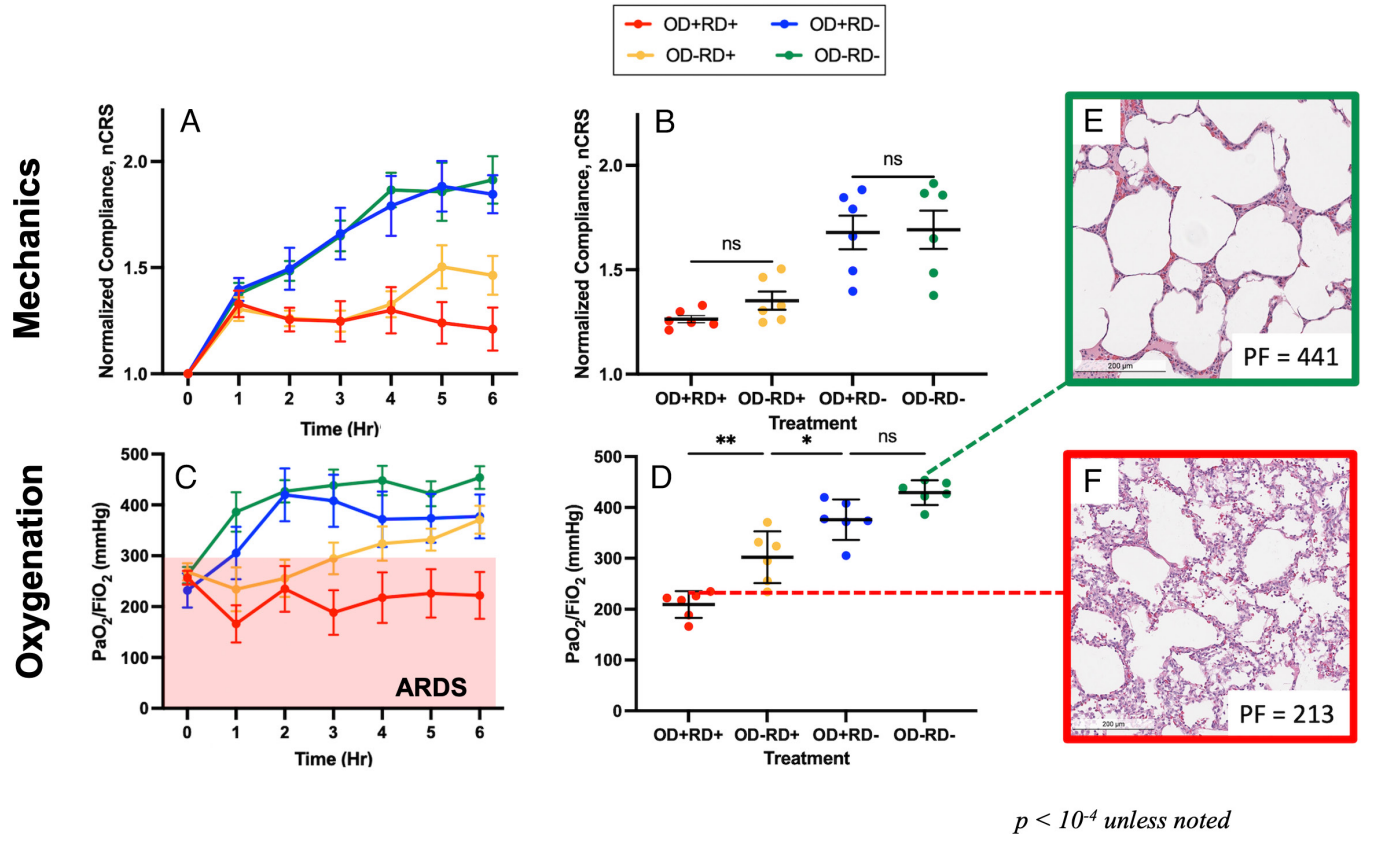

Fig. 3. Physiological measurements and their relationship to ventilation scenarios. Pulmonary mechanics assessed by normalized compliance (nC_{RS}) vs (*A*) time (T0–T6) and (*B*) treatment (T1–T6). Oxygenation was assessed by PaO_2/FiO_2 ratio vs (*C*) time (T0–T6), and (*D*) treatment (T1–T6). Histology represented for PaO_2/FiO_2 representative of (*E*) OD−RD−, and (*F*) OD+RD+. Time-course data (*A* and *C*) are represented as mean ± SEM for each time point. Treatment-based representation (*B* and *D*) symbols represent T1–T6 time-point means with error bars as treatment mean ± SEM. Each data point represents n =10 for OD−RD−, n = 7 for OD−RD+, n = 9 for OD+RD−, and n = 9 for OD+RD+ experimental subjects. ns = $P > 0.05$, *$P \le 0.05$, **$P \le 0.01$. Those not defined are all $P \le 0.0001$. Fig. 3 *A* and *C* reproduced with permission (22).

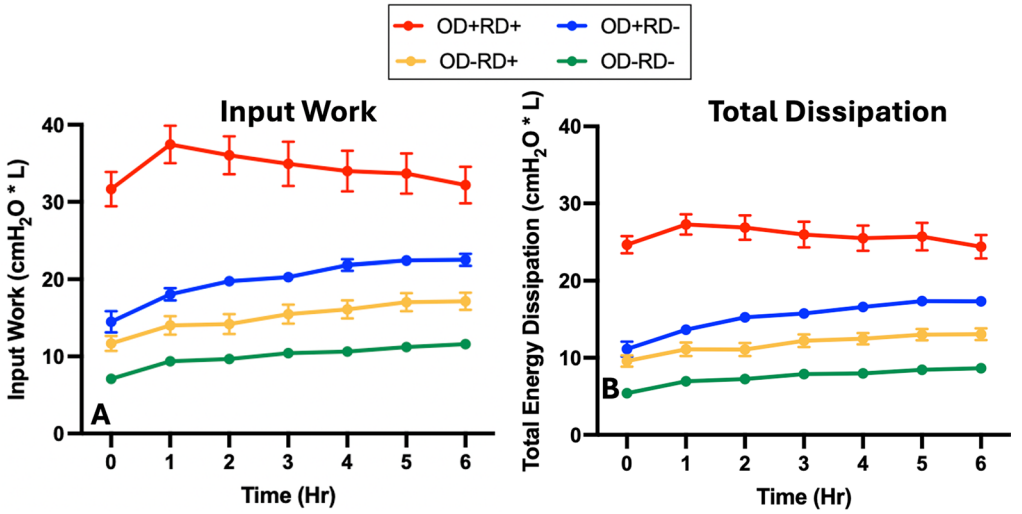

Fig. 4. (*A*) Input work vs time. (*B*) Total energy dissipation (D_{total}) vs time. Data are presented as mean ± SEM. Other statistics are described in Fig. 6.

from our previous study (22) in which the same animals were used for a different investigation).

Fig. 3 *E* and *F* presents histology images from OD–RD– and OD+RD+ experiments, respectively. Images from the diaphragmatic lobes exposed to the Tween injury were selected from animals with a final PaO_2/FiO_2 ratio reflecting the group means. These representative images demonstrate OD–RD– with relatively open alveoli, minimal edema/fibrin accrual, and no leukocyte infiltration, but with some capillary congestion (Fig. 3*E*). By comparison, the OD+RD+ group reveals accrual of edema with white and red blood cells within the alveolar air space (Fig. 3*F*). Furthermore, the OD+RD+ histology demonstrates relatively greater atelectasis with increased wall thickening.

In the energy analysis presented below, it is important to recognize the ranking of the physiological recovery response to injuries ranged from most to least severe as OD+RD+, OD–RD+, OD+RD–, OD–RD–, as illustrated in Fig. 3*D*. Of particular significance is the observation that animals experiencing RD alone (OD–RD+) exhibited both significantly reduced compliance ($P < 0.001$) and significantly greater impairment in oxygenation ($P = 0.0123$) compared to those with OD alone (OD+RD–). As we will illustrate, this finding plays a pivotal role in identifying mechanisms of energy dissipation that could potentially contribute to VILI.

Respiratory Mechanics. Pressure vs volume (PV) curves (*SI Appendix*, Fig. S2) reveal the distinguishing characteristics of the PV loops for four treatment groups: RD–OD–, OD+RD–, OD–RD+, and OD+RD+. These loops were evaluated to determine the levels of energy delivery and dissipation and their association with physiological function.

Total Input Work and Total Dissipation. Total input work and total dissipation are presented in Fig. 4. OD, and especially the combination of RD and OD, resulted in the greatest total energy input during inspiration (Fig. 4*A*), but this does not consider the energy recovered during expiration. The total energy dissipated during the complete ventilation cycle is given by the PV loop hysteresis area, D_{total} (Fig. 4*B*). The time-course trends of input and dissipated energy are identical, although D_{total} is smaller because it does not include recoverable elastic energy stored in the lung at the end of inspiration.

Dissipated Energy Components. Fig. 5 illustrates the dissipated energy components, which sum to the values of D_{total} shown in Fig. 4*B*.

$D_{airflow}$ for the four treatment groups (Fig. 5*A*) demonstrates trends that are nearly identical to those of D_{total}, with 76 to 88% of the total energy dissipation coming from airflow, likely due in

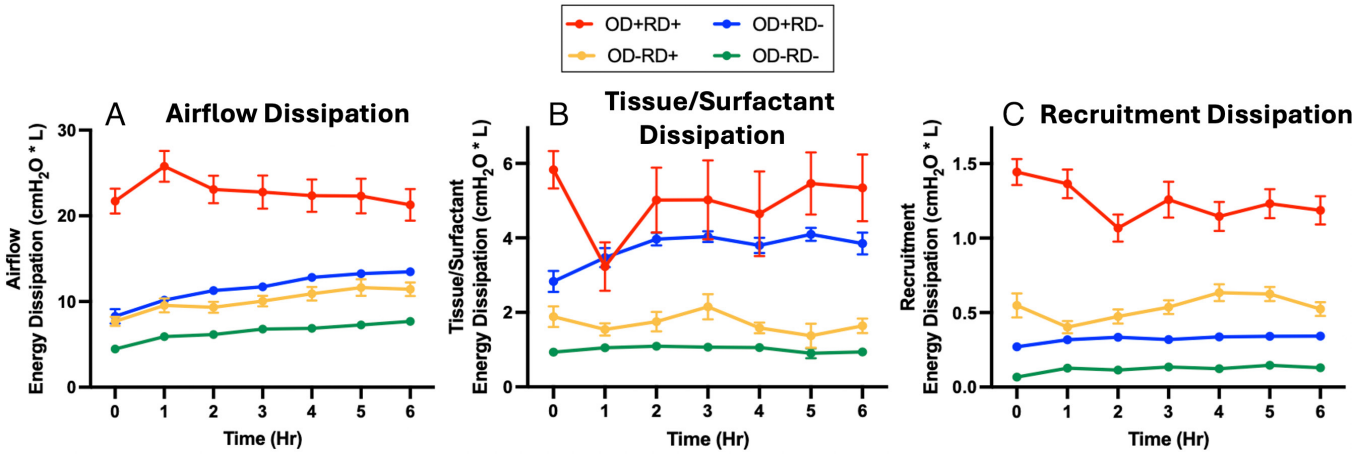

Fig. 5. Dissipation components vs time. (*A*) Airflow dissipation ($D_{airflow}$), (*B*) tissue/surfactant dissipation (D_{tissue}), and (*C*) recruitment dissipation ($D_{recruit}$). Data are presented as mean ± SEM. Additional statistics are described in Fig. 7.

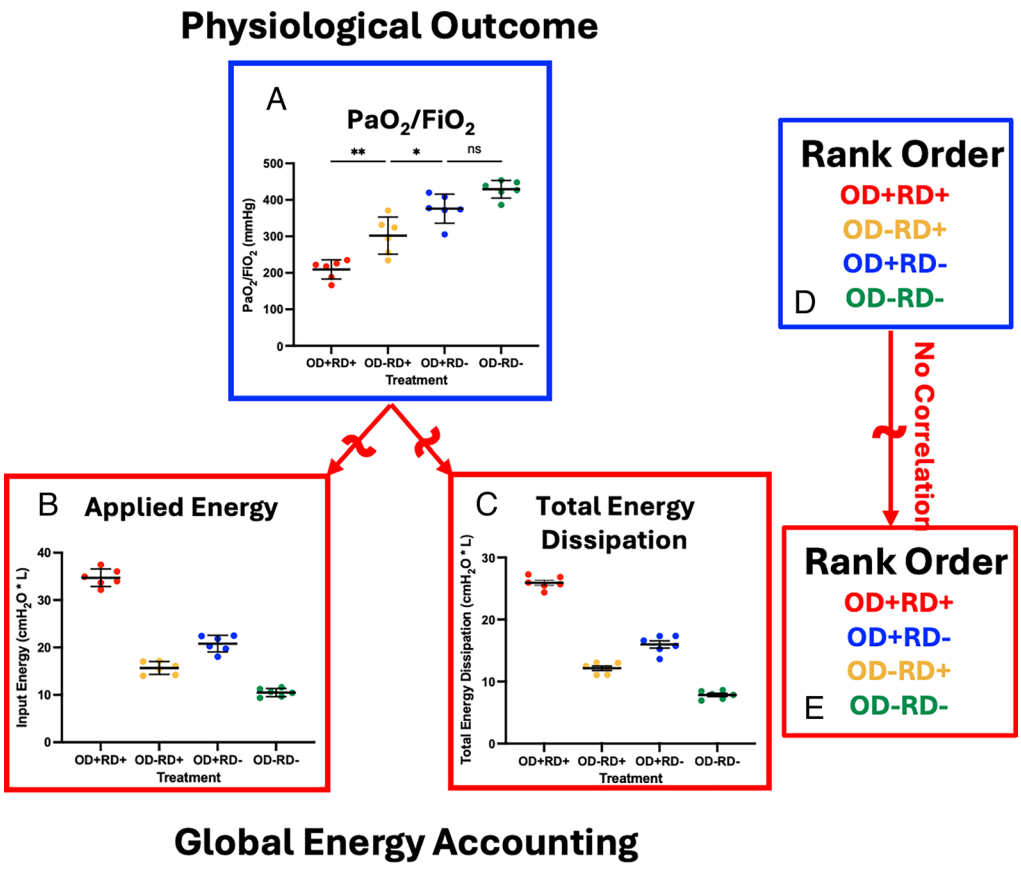

Fig. 6. Correlation analysis of physiological outcome to overall energy delivery and dissipation. Comparison of the treatment-based (*A*) PaO_2/FiO_2 physiological outcome (from Fig. 3*D*) to the (*B*) applied energy and (*C*) total energy dissipation from Fig. 4. The (*D*) physiological rank-order response demonstrates no correlation with the (*E*) applied energy and total energy dissipation rank-orders, indicating that these cannot be responsible for the physiological response. Symbols represent T1–T6 time-point means, and error bars represent treatment mean ± SEM. ns = $P > 0.05$, *$P \le 0.05$, **$P \le 0.01$. Those not defined are $P \le 0.0001$.

large part to turbulent flow in the proximal airways, with a smaller contribution from laminar flow more distally (23).

D_{tissue} was 14 to 24% of D_{total} and was substantially larger in the OD+ groups compared to the OD− groups (Fig. 5*B*). This dissipation component occurs in all ventilated regions, though there may be heterogeneous contributions due to differences in regional expansion.

$D_{recruit}$ was only 2 to 5% of D_{total} (Fig. 5*C*). This dissipation occurs only in those regions where airway/alveolar walls are separated by a finger of air that penetrates a liquid obstruction that holds walls in apposition (34–40) or by liquid plugs that propagate through the vessels (18, 41–45).

Correlation Analysis. We use the above data (Figs. 3–5) to identify a correlation between the manifestation of ARDS/VILI and the potential sources of applied energy and energy dissipation. We used oxygenation as the reference biomarker of lung injury, noting that it is consistent with mechanical compliance measurements and previous histological observation (11) as shown in Fig. 3 *E* and *F*.

Global energy. Fig. 6 compares the treatment data between A) PaO_2/FiO_2 (from Fig. 3*D*) and B) inspiration energy (from Fig. 4*A*), and C) total dissipated energy (from Fig. 4*B*). From this comparison, the physiologic rank order (Fig. 6*D*) does not correlate with the rank order of either inspiration or total dissipated energy (Fig. 6*E*). In particular, the energies are less for OD−RD+ than for OD+RD−, even though OD−RD+ is more physiologically impactful than OD+RD−. This correlation analysis demonstrates that neither total applied energy nor total energy dissipation can explain the physiological impact of VILI.

Dissipated energy. Fig. 7 makes a corresponding comparison between the physiological response based on oxygenation (PaO_2/FiO_2 from Fig. 3*D*) and each of the subcomponents of energy dissipation (from Fig. 5). By comparing the physiological rank order (Fig. 7*E*) to the rank order of airflow and tissue-level dissipation (Fig. 7*F*), we can see that no correlation exists. In contrast, the rank order of recruitment dissipation (Fig. 7*G*) is consistent with the physiological response rank order (Fig. 7*E*). Among the analyzed components of energy dissipation, only the one due to RD shares the same rank order as the physiological response (Fig. 7*D*), implying that recruitment derecruitment dissipation is the only energy component that can be directly linked to VILI.

Statistical and Time-Course Analysis. The correlation analysis above provides evidence that the oxygenation response is aligned only with recruitment energy dissipation. This relationship also holds for the mechanical recovery, nC_{RS}. Fig. 8 further elucidates the statistical and temporal relationships between oxygenation and mechanics as a function of $D_{recruit}$.

Fig. 8 *A*–*C* demonstrates that reduced recruitment energy dissipation ($D_{Recruit}$) is correlated with improved oxygenation (PaO_2/FiO_2) and mechanical recovery (nC_{RS}). First, Fig. 8*A* demonstrates that the initial PaO_2 is impaired for all treatment cases, validating that the initial lung injury is independent of the treatment modality, with all groups experiencing a significant decrease in oxygenation. In comparison, Fig. 8*B* illustrates that at T6 a dose-dependent relationship exists between $D_{Recruit}$ and oxygenation recovery. Importantly, the behavior observed at T0 (initial state) to T6

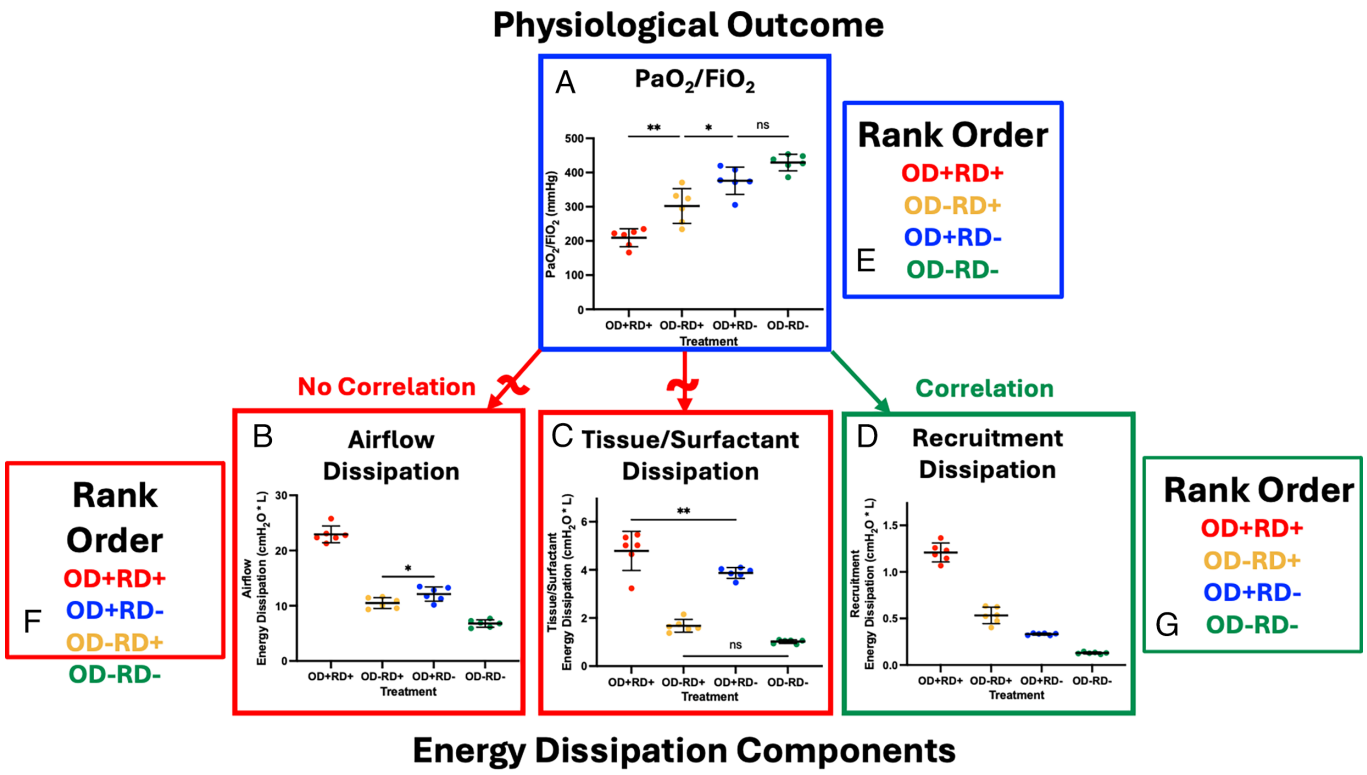

Fig. 7. Correlation analysis of physiological outcome to energy dissipation components. Comparison of the (*A*) PaO_2/FiO_2 physiological outcome (from Fig. 3*D*) to the (*B*) airflow dissipation, (*C*) tissue energy dissipation, and (*D*) recruitment dissipation from Fig. 5, respectively. The (*E*) physiological rank-order response demonstrates that no correlation exists between the (*F*) rank order of airflow and tissue dissipation, indicating that these cannot be responsible for the physiological response. In contrast, the (*E*) physiological rank-order correlates with the rank order of (*G*) recruitment dissipation, indicating that recruitment dissipation can be responsible for VILI. Symbols represent T1–T6 time-point means, and error bars represent treatment mean ± SEM. ns = $P > 0.05$, *$P \le 0.05$, **$P \le 0.01$. Those not defined are all $P \le 0.0001$.

improves oxygenation recovery at lower $D_{Recruit}$ levels (Fig. 8*B*). A linear regression of the T6 response gives the relationship:

$$\frac{PaO_2}{FiO_2} = 480\,mmHg - 237\frac{mmHg}{cmH_2O * L}D_{recruit}, R^2 = 0.32. \quad [1]$$

Statistical analysis illustrated by the 95% confidence range shows that the regression slope is many SE from the zero-slope null hypothesis ($P = 0.0001$). This provides significant evidence in favor of the hypothesis that low levels of $D_{Recruit}$ are associated with injury recovery.

Fig. 8*C* further elucidates the temporal dose-dependent recovery transition. OD–RD– and OD+RD– recovery is swift at low $D_{recruit}$ ($D_{recruit} < 0.4$ cmH_2O*L), with significant slopes ($P = 0.0001$ and $P = 0.009$, respectively), demonstrating robust recovery. OD–RD+ provides intermediate values of $D_{recruit}$ (0.4 cmH_2O*L < $D_{recruit}$ < 1.0 cmH_2O*L), with recovery following a more tempered pace, but a significantly nonzero slope ($P = 0.009$), illustrating the continuation of the dose–response behavior. Conversely, oxygenation recovery does not exist with $D_{Recruit} > 1$ cmH_2O*L (OD+RD+), and thus, we cannot dismiss the null hypothesis ($P = 0.9$) at large values of $D_{Recruit}$.

Similar dose-dependent recovery patterns are observed for mechanics (nC_{RS}) (Fig. 8 *D* and *E*). Reduced $D_{Recruit}$ is associated with improved nC_{RS} recovery. Fig. 8*D* shows the linear regression relationship:

$$nCRS = 2.0 - \frac{0.7}{cmH_2O * L}D_{recruit}, R^2 = 0.47. \quad [2]$$

Statistical analysis illustrated by the 95% confidence range is consistent with the hypothesis that low levels of $D_{Recruit}$ are associated with injury recovery ($P < 0.0001$).

Fig. 8*E* further elucidates the temporal dose-dependent recovery of nC_{RS} in a manner equivalent to that illustrated by oxygenation (Fig. 8*C*). Treatments with lower $D_{recruit}$ ($D_{recruit} < 0.4$ cmH_2O*L), display significant recovery with nonzero slopes ($P = 0.007$ and $P < 0.0001$, respectively). Intermediate values of $D_{recruit}$ (0.4 cmH_2O*L <$D_{recruit}$ < 1.0 cmH_2O*L) provided by OD–RD+ indicate a positive, but potentially not significant, recovery trend ($P = 0.09$). Like oxygenation, high $D_{Recruit}$ treatment (OD+RD+, $D_{recruit} > 1$ cmH_2O*L (OD+RD+), does not exhibit significant compliance recovery, and we cannot dismiss the null hypothesis ($P = 0.09$) at large values of $D_{recruit}$. This indicates that injury continues at high levels of $D_{recruit}$.

In summary, the physiological responses quantified by oxygenation and pulmonary mechanics illustrate significant dose–response relationships that correlate significantly with energy dissipation from airway/alveolar recruitment only. We thus hypothesize that this form of energy dissipation should be minimized to prevent VILI.

Biomedical Engineering Analysis: Dissipation Modeling at the Alveolar Level. It is perhaps surprising that the injurious component of dissipated energy, that due to alveolar/airway reopening, is so small. A possible explanation for the damaging nature of reopening is that it is focused on specific and very small regions of tissue. Dissipation by reopening occurs only in regions where airway/alveolar walls are held together in apposition due to surface tension, or by liquid plugs that block airflow and create a compliant collapse configuration. Energy dissipation occurs when a finger of air forces the walls apart (34–40), or the plug is removed through meniscus rupture (18, 41–45). These are highly localized events. Furthermore, these events take place over very short time intervals because alveoli

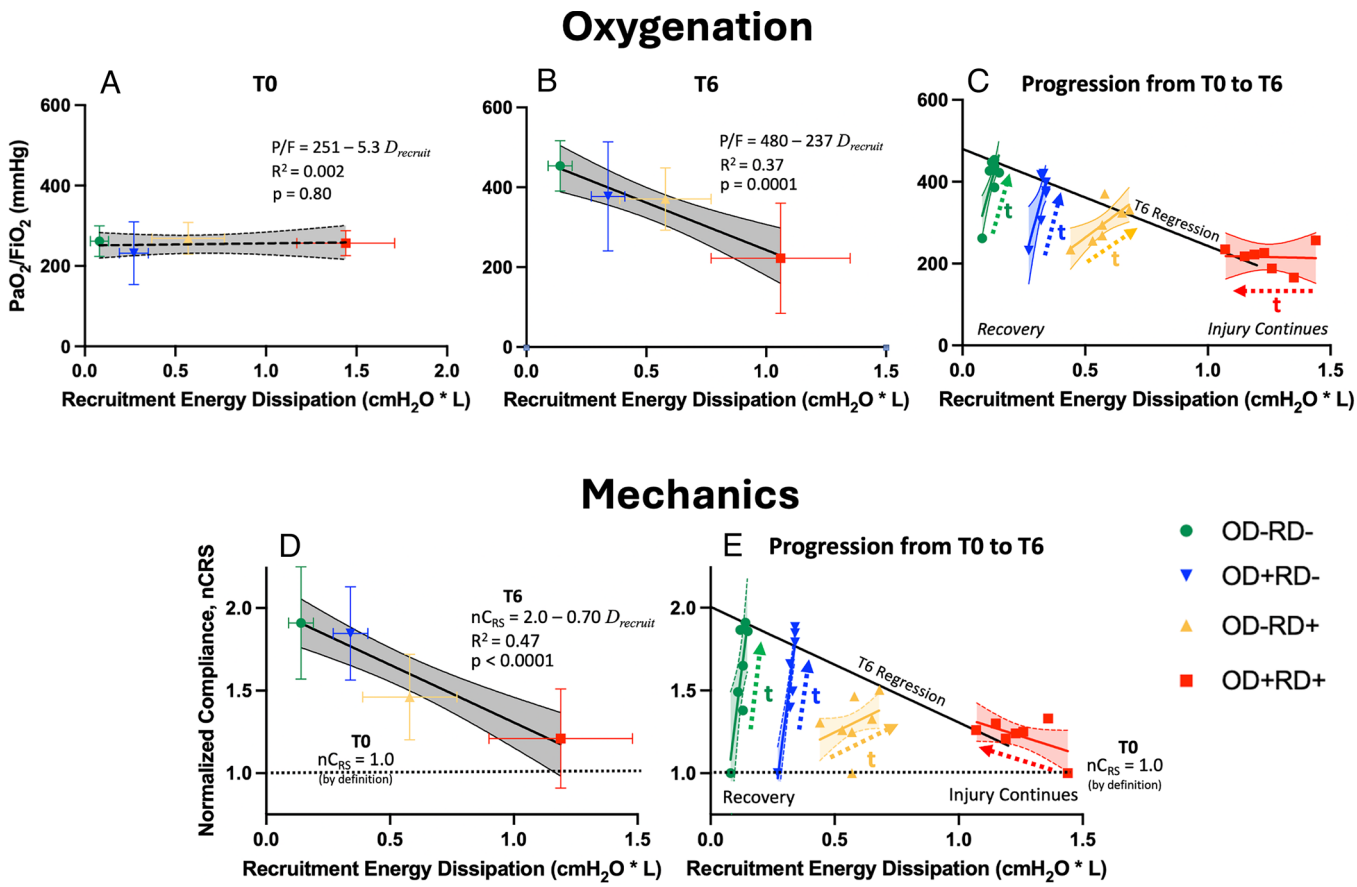

Fig. 8. Relationships between recruitment energy dissipation and physiological responses from T0 to T6 demonstrate recovery only for low levels of recruitment dissipation. Physiological responses [*A–C*: oxygenation (PaO_2/FiO_2) and *D* and *E* mechanics (nC_{RS})] to recruitment energy dissipation $D_{Recruit}$. (*A*) Initial oxygenation is independent of the treatment modality; (*B*) T6 recovery of oxygenation demonstrates that recovery is dependent on $D_{Recruit}$; (*C*) Oxygen recovery for each treatment demonstrates recovery for low $D_{Recruit}$ and continued injury for large $D_{Recruit}$. (*D*) Mechanics at T0 and T6 demonstrating compliance recovery is dependent on $D_{Recruit}$; (*E*) nC_{RS} recovery transition for each treatment demonstrates recovery for low $D_{Recruit}$ and continued injury for large $D_{Recruit}$. Shaded regions represent 95% CI. Data in *A*, *B*, *D*, and *E* represent mean ± SD. Data in *C* and *E* represent mean values for T0–T6.

and airways transition between open and closed states in small fractions of a second. These factors potentially give rise to a *high dissipation power intensity* that may initially cause small areas of local damage from which injury then propagates (46). In contrast, dissipation due to gas flow in airways and stretch of viscoelastic tissues occur everywhere throughout the lung and so likely have smaller dissipation power intensities despite having larger overall magnitudes.

To quantify the power intensity due to recruitment, we consider the amount of energy dissipation from the recruitment of a single alveolus. To evaluate dissipation per alveolar recruitment event, we consider the work done in inflating a single collapsed alveolus to a fully inflated sphere of radius R through application of a pressure P, given by

$$E_{recruit} = P\Delta V. \quad [3]$$

Since $E_{recruit}$ is required to overcome the surface tension forces holding the alveolus in a collapsed state, it represents an estimate of the energy dissipated to break those forces. The reopening pressure P is related to surface tension, γ, and is inversely related to R following the Law of Laplace,

$$P = \frac{K\gamma}{R}, \quad [4]$$

where K ~ 10 or larger depending on the recruitment speed (34, 47). So, assuming a spherical alveolus, the approximate energy dissipation from a recruited alveolus is

$$E_{recruit} = \frac{4}{3}\pi K\gamma R^2. \quad [5]$$

For a moderately elevated surface tension (γ = 30 dyn/cm), and an alveolar radius in the range 5×10^{-3} cm ≤ $R \leq 1 \times 10^{-2}$ cm, the estimate for energy dissipation from a single recruitment event is estimated as

$$3.14\frac{nJ}{alv} \leq E_{recruit} \leq 12.6\frac{nJ}{alv}, \quad [6]$$

where the lower bound represents the energy needed to recruit an alveolus near RV while the upper bound is the energy to recruit an alveolus near TLC.

The dissipated power is defined as $Power_{recruit} = \frac{E_{recruit}}{T_{recruit}}$, where $T_{recruit}$ is the recruitment time. Since the auditory spectrum for fine crackles in the lung occurs over the kilohertz range (48, 49), recruitment events occur over a timescale of $T_{recruit} \sim 10^{-3}s$. The power dissipated by recruitment of a single alveolus is thus in the range

$$3.14\frac{\mu W}{alv} \leq Power_{recruit} \leq 12.6\frac{\mu W}{alv}. \quad [7]$$

This gives the recruitment dissipation power intensity for a single alveolus (that is, the rate of energy dissipation per unit area applied to the epithelial surface) as

$$I_{recruit} \sim 10^{-2}\frac{W}{cm^2} = 100\frac{\mathrm{W}}{\mathrm{m}^2}. \quad [8]$$

This result is independent of the timing during the breathing cycle, as recruitment at RV has a smaller dissipation energy than at TLC, but this is distributed over a smaller area as well.

For context, we analyzed the power intensity from tissue stretch, using our measurements from OD+RD+ (Fig. 7*C*) as

$$D_{stretch} \sim 5cmH20 * L = 0.5\text{J}, \quad [9]$$

where we assume that the majority of $D_{stretch}$ occurs at the alveolar level, with an alveolar surface area for a 38.3 kg pig (the average of this study) as $A_{alv} = 93m^2$ (50). Furthermore, this dissipation occurs at end inspiration over a time range from $0.1s \leq t_{stretch} \leq 1s$. This gives the tissue stretch dissipation power intensity as

$$5.4 \times 10^{-3} \frac{\text{W}}{\text{m}^2} \leq I_{stretch} \leq 5.4 \times 10^{-2} \frac{\text{W}}{\text{m}^2}. \quad [10]$$

In a "baby lung" scenario (51) the power intensity could be greater owing to the smaller surface area of communicating alveoli. Nevertheless, the above calculation indicates that pure stretching of tissues, while providing a larger net dissipation, provides regional power intensity that is many orders of magnitude smaller than that from highly focused recruitment events (Eq. **8**).

For further context, the irradiance of sunlight onto the Earth's surface at high noon is $I_{sun} \sim 1{,}000 \frac{W}{m^2}$ (52), so the power intensity associated with energy dissipation due to alveolar recruitment is equivalent to that of solar energy at dawn or dusk, or on a cloudy day. Such power intensity is perhaps not normally associated with damage to the skin, but when applied to the delicate pulmonary epithelium over hours of mechanical ventilation, it might well cause significant damage.

Recruitment Magnitude. The total RD energy dissipated during a breath is the product of E_{recuit} (Eq. **8**) and the total number of alveoli, $NAlv_{recruit}$, that become recruited. This gives

$$NAlv_{recruit} = \frac{D_{recruit}}{E_{recrut}}. \quad [11]$$

The Table 1 provides $NAlv_{recruit}$ for each of the four treatment modalities. It is notable that the number of recruited alveoli for the most harmful modalities (OD+RD+ and OD–RD+) is 5 to 10 times larger than those for the protective modalities (OD+RD– and OD–RD–). The rapid recoveries from injury seen with the OD+RD– and OD–RD– treatments (Figs. 3 *A* and *C* and 8 *C* and *E*) suggest that there is a critical level of recurring injury that can be endured without causing a catastrophic decline in organ-level function. The critical breakpoint is approximately 5 to 10 million recruitment events per cycle for the surfactant deactivation injury model examined in this study. This breakpoint may vary for different causes of ARDS. Nonetheless, the above analysis suggests that the total number of cyclically recruited alveoli per breath may be the most crucial predictor of VILI.

Table 1. Estimated number of alveoli recruited ($NAlv_{recruit}$) and approximate volume associated with the recruited alveoli (V_{NAlv})

	$NAlv_{recruit}$ (million alveoli)	V_{NAlv} (ml)	$V_{recruit}$ (ml)	$\%_{recruit}$(%)
OD+RD+	10 to 40	20 to 40	400	5 to 10
OD–RD+	4 to 16	8 to 16	200	4 to 8
OD+RD–	2.4 to 12	5 to 10	200	2.5 to 5
OD–RD–	0.8 to 4	1.7 to 3.4	175	1 to 2

The volume of the lung related to the recruitment phase ($V_{recruit}$) allows for the estimate of the percentage of alveoli ($\%_{recruit}$) that are engaged in recruitment/derecruitment events.

Discussion

We used APRV to independently control OD and RD in the lung in a porcine ARDS model and found that approximately 20% of the delivered energy was elastic energy that was recovered during exhalation, while the rest was dissipated. Of the dissipated energy, 76 to 88% was dissipated through airflow, 14 to 24% through tissue-level dissipation, and only 2 to 5% was dissipated through RD. Pulmonary mechanics quantified by normalized compliance (n_{CRS}) and functional oxygenation (PaO_2/FiO_2) provided biomarkers of lung injury, with the rank order of physiological outcomes from worst-to-best being: 1) OD+RD+, 2) OD–RD+, 3) OD+RD–, and 4) OD–RD–. Only the measured component of energy dissipated by alveolar/airway reopening ($D_{recruit}$) correlated with this physiological response, suggesting that dissipation from alveolar/airway reopening is directly related to the generation or persistence of VILI while the other components of dissipated energy are not.

The correlation between RD and VILI is a significant result, especially given the fact that only a small fraction of energy dissipation (2 to 5%) is caused by these events. To elucidate the biomechanics of this process, we estimated the power intensity of RD events using theoretical and computational analyses (34, 35, 53). We found that intensity from RD is approximately 100 W/m^2, which is many orders of magnitude greater than that due to tissue stretch. This large power intensity results from RD being highly localized, and of very short duration, acting like an explosive event at the epithelial surface. In vitro RD studies have demonstrated direct cell damage and barrier function disruption (36, 38), which can lead to cascading lung instability associated with VILI (46, 54, 55). Our calculations also demonstrate the likelihood that the lung can recover if RD is reduced below a critical value. This opens the door for adaptive personalized ventilation that can reduce the severity of VILI and lead to recovery.

We used oxygenation (PaO_2/FiO_2) and mechanics (nC_{RS}) to assess injury recovery/progression as a function of treatment modality. PaO_2/FiO_2 is not only affected by lung injury but also potentially by cardiovascular factors. We showed in our previous study (22), however, that heart rate, cardiac output, and global end-diastolic volume were similar among the treatment groups. We also showed histologically that the OD+RD+ group had a significant increase in fibrin accumulation and leukocyte infiltration with a relative increase in red blood cells, whereas the OD–RD– group had a significant decrease in air space leukocytes (22). These complementary approaches thus support the validity of using PaO_2/FiO_2 to evaluate the impact of energy delivery and dissipation on lung injury.

It is important to note that while these data suggest irreparable lung damage results from energy dissipation due to reopening of closed lung units, they cannot eliminate the impact of OD on lung injury. Recent studies by Ghadiali and colleagues indicate that atelectrauma is more damaging than volutrauma and that barrier disruption during simultaneous volutrauma and atelectrauma is driven by atelectrauma (56). Our data make it clear that OD combined with RD (OD+RD+) is more damaging than RD alone (OD–RD+). OD may potentiate more injurious RD by

increasing the tissue tension near regions of closure, which substantially increases microscale biomechanical stresses (35). Furthermore, when considering the traditional approaches targeting the RD component of VILI, such as recruitment maneuvers and the open lung approach, none have demonstrated a clear benefit and may, in fact, pose risks (55, 57, 58). It is plausible that opening the lung without maintaining a sustained and stable inflation could increase localized RD energy dissipation. An alternative approach could entail a more deliberate stabilization of the lung to abrogate this highly focalized injurious component.

There are several limitations to this study that should be considered. First, our analysis relies on a calculation of airway resistance to determine the component of energy related to dissipation from airflow, and thus to determine the quasi-steady alveolar-level PV loop. We assumed airway resistance was equal to R_{rs} and that this value remained constant throughout the ventilatory cycle. In reality, airway resistance changes throughout the ventilation cycle. We also assumed that the recruitment energy can be determined from the inflation limb of the alveolar PV relationship prior to its true inflection point. This region is associated with audible crackles that are indicative of recruitment (59), and the sharp increase in compliance in that region is also strongly suggestive of significant recruitment events. Nevertheless, the PV area determined from the linear extrapolation of the PV loop to the beginning of inspiration is only a first-order approximation of the recruitment energy dissipation and likely is an overestimate. Likewise, the remainder of the PV loop, after subtraction of airflow and recruitment contributions, is attributed entirely to tissue-level dissipation (including energy loss from dynamic surface tension), which again is an approximation. Despite these limitations, however, the absence of a statistical difference in tissue-level dissipation between the two OD− cases, and the similarity of the two OD+ cases, suggests that our analysis of the PV relationships was a reasonable first approximation.

Finally, the clinical relevance of our study may be limited by an ARDS model that involves a one-time localized delivery of a 3% Tween-20 detergent solution into only the dependent basilar lung regions, which deactivates surfactant in that region. While surfactant deactivation is a key characteristic of ARDS, this is not typical of the initiation of ARDS clinically, which may involve systemic causes such as sepsis. Nevertheless, ARDS from other causes eventually results in barrier-function dysregulation (60) that results in surfactant deactivation (55), so our model recapitulates a key endpoint common to ARDS in general.

While both overdistension (OD) and recruitment/derecruitment (RD) have been broadly implicated in VILI, their precise initiation and relative contributions have remained unclear. This study introduces an impedance measurement tool and algorithm that enables the evaluation of energy delivery and dissipation. By correlating these measurements with the physiological responses of a mechanically ventilated pig model of ARDS, we quantify energy delivery and dissipation due to airflow, tissue deformation, and alveolar/airway recruitment. This approach elucidates the physiological significance of OD and RD, providing a clearer understanding of their roles in VILI.

The only component of energy dissipation that correlated to reduced physiological recovery was recruitment, even though only 2 to 5% of the total energy dissipation was attributed to that component. We estimate that the energy dissipation from a single recruitment event is very low (~10 nJ). Nevertheless, the dissipation from such an event occurs over a very short timescale and is applied to a tiny surface area. This results in a dissipation power intensity estimated to be 100 W/m^2. We also found that recovery from ARDS was rapid if the total recruitment dissipation energy was low, but recovery did not occur when 5 to 10% of alveoli underwent repetitive RD. Our findings suggest that energy dissipation due to recruitment during inspiration is the primary cause of VILI, implying that it is crucial to minimize recruitment and derecruitment events during mechanical ventilation of the injured lung. A personalized mechanical ventilation approach using the detection methods described herein may help reduce VILI and, consequently, lower the mortality rate of ARDS.

Materials and Methods

Experiments were conducted with approval from the SUNY Upstate Medical University IACUC following ARRIVE guidelines as described in our previous studies that used data from the same animals (22). The experimental setup is described in Fig. 9. ARDS was generated in female Yorkshire pigs ($n = 40$, 38.3 ± 1.8 kg) as follows (61). The animals were anesthetized with intravenous ketamine (90 mg/kg) and xylazine (10 mg/kg) and paralyzed with rocuronium. Next, continuous positive airway pressure (CPAP) was applied while 3% Tween-20 was instilled into the bilateral-dependent basilar lung regions (0.75 mL/kg into each side). Tween-20, a detergent, disrupts the natural surfactant layer, resulting in increased surface tension, alveolar collapse, and impaired gas exchange (62). This disruption triggers an inflammatory response that damages the alveolar-capillary barrier, increasing its permeability and causing fluid leakage into the alveoli. Consequently, this damage hinders the lungs' ability to oxygenate blood and remove carbon dioxide, thereby mimicking the clinical features of ARDS (22, 55, 63).

Ventilation Protocols. Following injury, the animals were randomly divided into four groups OD+RD+, OD+RD−, OD−RD+, and OD−RD− according to whether they were protected from or subjected to overdistention (OD+ and OD−, respectively), and similarly for recruitment and derecruitment (RD+ and RD−, respectively). To accomplish this, the animals were ventilated with airway pressure release ventilation (APRV) because this allowed independent control of OD and RD as follows (64, 65)

1) OD determined by inspiration pressure: (P_{High}):
   - OD+ by setting $P_{High} = 40$ cmH_2O, leading lung overdistension (63),
   - OD− created by setting $P_{High} = 28$ cmH_2O, since this is below the plateau pressure limit suggested by clinical guidelines (4),
2) RD determined by expiration duration (T_{Low}):
   - RD+ by prolonged exhalation through termination when end-expiratory flow had fallen to 25% of its early peak expiratory flow rate, resulting in $T_{Low} \sim 1$ s.
   - RD− created by short exhalation by terminating expiration when end-expiratory flow had fallen to only 75% of its early peak expiratory flow rate, resulting in $T_{Low} \sim 0.5$ s.

Representative tracheal pressure and flow waveforms from the four groups of animals are shown in *SI Appendix*, Fig. S1. A power analysis was conducted using statistics from of a similar animal model (63). We thus planned for $n = 10$ per group, using alpha = 0.05 and power = 90%. Dropout due to technical issues resulted in $n = 10$ for OD−RD−, $n = 7$ for OD−RD+, $n = 9$ for OD+RD−, and $n = 9$ for OD+RD+.

Oxygenation/Physiologic Monitoring. Continuous monitoring of oxygen saturation, mean arterial pressure (MAP), heart rate, and temperature was performed (IntelliVue MP90, Philips Healthcare, Irvine, CA). Arterial blood gases and electrolyte concentrations were measured every hour (pH, PaO_2, PCO_2, oxygen saturation, sodium, potassium, chloride, calcium, and PaO_2/FiO_2 ratio). Ventilatory parameters (peak inspiratory pressure, mean airway pressure, plateau pressure, tidal volume, resistance, P_{High}, P_{Low}, T_{High}, and T_{Low}) were also acquired hourly. The VolumeView™ system provided estimates of cardiac output, extravascular lung water, and global end-diastolic volume. Driving pressure (ΔP) was calculated as the difference between the plateau pressure and positive end-expiratory pressure. These data have been reported previously (22) though not in the context of the present study. Here, we focus on oxygenation reflected in PaO_2/FiO_2 as a key measure of physiologic health, with $PaO_2/FiO_2 < 300$ mmHg indicating ARDS (21).

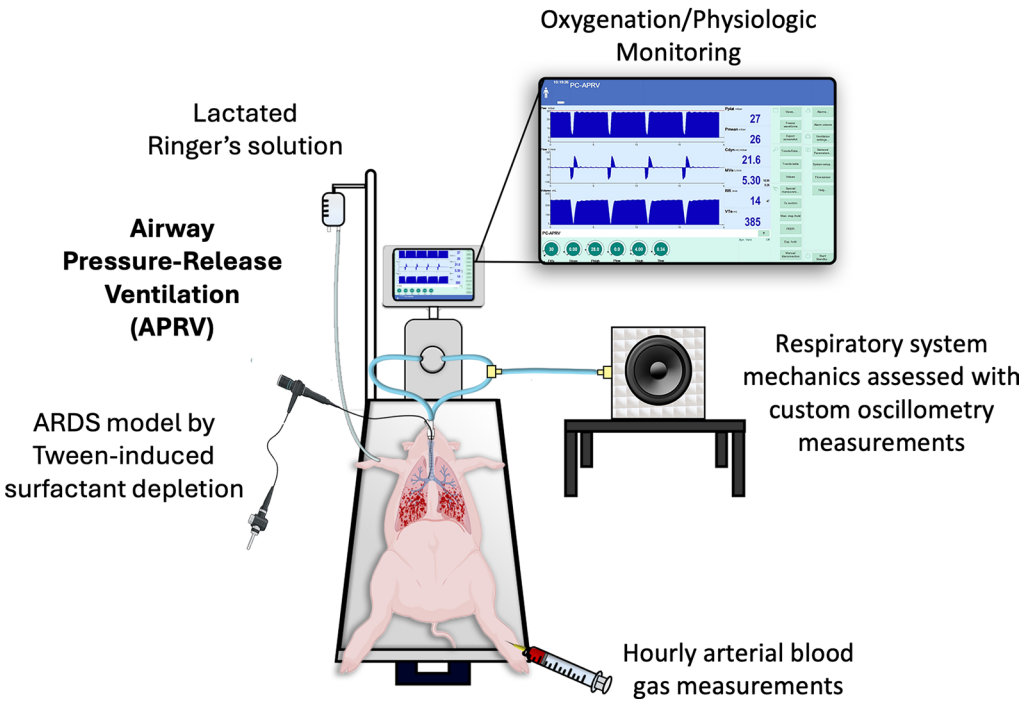

Fig. 9. Experimental setup: The ARDS pig model is ventilated with APRV as respiratory system mechanics and physiological systems are monitored for six hours postinjury. Created with BioRender.com.

Histology. Postmortem, tissue sections from the right diaphragmatic lobe (Tween-injured tissue) were excised and submerged in formalin for histopathologic analysis. Representative photomicrographs of diaphragmatic tissue sections are provided in Results (Fig. 3 *E* and *F*). Quantitative evaluations from these measurements are provided in (22).

Our prior analysis from these experiments demonstrated that OD−RD− significantly improves oxygenation and mechanics while reducing pulmonary edema, microvascular permeability, histopathology, and white blood cell infiltration, but without compromising hemodynamics (22).

Respiratory System Mechanics. The mechanical properties of the respiratory system were assessed using a custom oscillometry setup (22). Ten-second epochs of forced oscillatory flow were applied hourly for 6 h following Tween injury. Airflow ($\dot{V}$), tracheal pressure (P_{trach}), and esophageal pressure (P_{esoph}) as an estimate of pleural pressure were measured as functions of time (t) during each epoch. Respiratory impedance (Z) as a function of frequency (f) was calculated from the Fourier domain ratio of pressure to flow. $Z(f)$ was fit with a single-compartment resistance–elastance–inertance model (66) that provided values for respiratory system resistance (R_{RS}), elastance, and inertance. The biomechanical state of the respiratory tissues was assessed by respiratory system compliance (C_{RS}−−inverse of elastance). This physiological outcome measure is reflective of respiratory system mechanics. C_{RS} was normalized to each animal's value immediately following injury (nC_{RS}). These data have been reported previously (22) though not in the context of the present study. See *SI Appendix* for more details.

Respiratory Pressures. Energy calculations necessitate quantifying the time-dependent pressures within the lung (Fig. 10). Specifically, the alveolar pressure is approximated as $P_{alv} = P_{trach} - P_{airflow}$, where $P_{airflow}(t) = R_{RS}\dot{V}(t)$. The distending pressure at the tissue level is $P_{tissue}(t) = P_{alv}(t) - P_{esoph}(t)$. Details of these calculations are provided in *SI Appendix*.

Calculation of Input Work and Dissipated Energy. The total input work provided to the lung by the ventilator during inspiration is given by:

$$\text{Input Work} = \int_{V_{min}}^{V_{max}} P_{trach}\,dV = \int_{t_0}^{t_0+T_{inhale}} P_{trach}\frac{dV}{dt}\,dt = \int_{t_0}^{t_0+T_{inhale}} P_{trach}\dot{V}\,dt, \quad [12]$$

where V_{min} and V_{max} are the lung volumes at the beginning and end of inspiration, respectively. The tidal volume is given by $V_T = V_{max} - V_{min}$. Likewise, t_0 is the time of onset of inhalation, and T_{inhale} is the inhalation duration.

The energy dissipated within the lungs over a single complete breath is equal to the area enclosed by the pressure–volume loop (67). As such, the total dissipated energy per breath, D_{total}, is

$$D_{total} = \oint P_{tp}\,dV = \int_{V(t_0)}^{V(t_0+T)} P_{tp}\,dV = \int_{t_0}^{t_0+T} P_{tp}(t)\dot{V}\,dt = D_{airflow} + D_{tissue} + D_{recruit}, \quad [13]$$

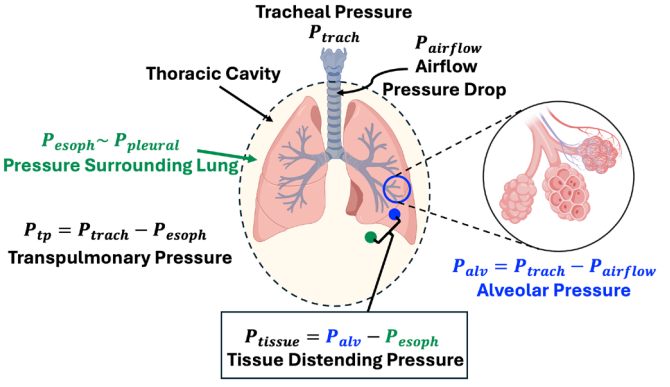

Fig. 10. Respiratory system pressures. Created with BioRender.com.

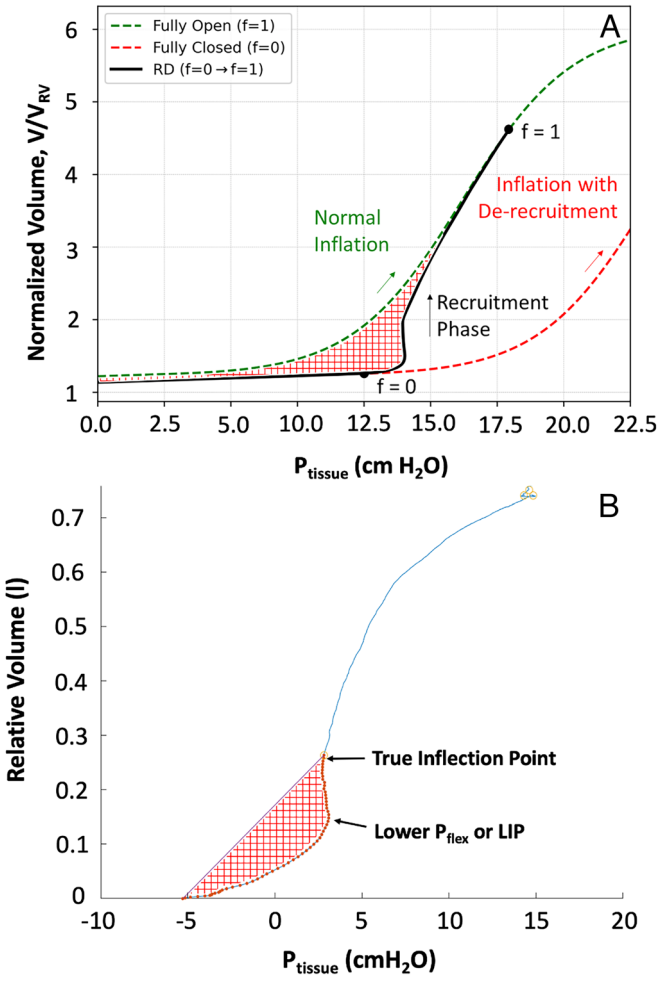

Fig. 11. (*A*) Computational model description of compliance recovery during recruitment. The green curve describes the PV relationship for a completely recruited acinus during inflation (f = 1), and the red curve describes the PV relationship for an ARDS derecruited acinus ($f \sim 0$). With recruitment, f increases, and the PV relationship undergoes a dynamic transition toward a healthy acinus (black solid curve). The red hashed region reflects the energy dissipation from the transition in states. Reproduced with permission (53). (*B*) The inflation limb of an experimental PV loop from this study, with the location of the true inflection point and the region associated with recruitment indicated in red.

where T is the duration of the breath (i.e., from the beginning of inspiration to the end of the subsequent expiration), and $D_{airflow}$, D_{tissue}, and $D_{recruit}$ are the amounts of energy dissipated by airflow, tissue movement, and RD, respectively.

We calculated D_{total} from the area of the PV loop using the transpulmonary pressure, $P_{tp}(t) = P_{trach}(t) - P_{esoph}(t)$. The three components of D_{total} correspond to distinct regions of the PV loop as illustrated in Fig. 2. These regions were identified as follows:

- $D_{airflow}$: We assume that R_{rs} approximates airway resistance, so the pressure drop across the pulmonary airways is $P_{airflow}(t) = R_{rs}\dot{V}(t)$. The time-integral of $P_{airflow}(t) * \dot{V}(t)$ then determines $D_{airflow}$.
- $D_{recruit}$: At the acinar level, the dissipation region from airway/alveolar recruitment can be understood from the inflation limb of the PV loop. Fig. 11*A* illustrates this as the dynamic transition from a derecruited state ($f \sim 0$ in red) with very low compliance [a "baby acinus," (51)], to the recruited state ($f = 1$ in green). Following the computational analysis of (53), the black curve represents the dynamic switch, and the shaded area reflects the recruitment energy dissipation for that subacinar region.

Accordingly, we assessed the inflation limb of the experimental $P_{tissue}(t)$ vs $V(t)$ loops, where $P_{tissue} = \left(P_{trach}(t) - R_{rs}\dot{V}(t)\right) - P_{esoph}(t)$ approximates the pressure drop across the lung parenchymal tissues (Fig. 11*B*). To calculate $D_{recruit}$, we identified the lower pressure inflection point, P_{flex}, as the start of alveolar recruitment (68). $D_{recruit}$ was taken as the area of the region with upward concavity. A detailed description of this area calculation is provided in *SI Appendix*.

- D_{tissue}: Finally, $D_{tissue} = D_{total} - D_{airflow} - D_{recruit}$.

Statistical Analysis. Descriptive statistics are reported as mean and SE for temporal results and mean and SE for treatment comparisons. Repeated measures ANOVA was used to compare treatment groups. Analysis was performed using Prism 10 (GraphPad Software, Ca).

Data, Materials, and Software Availability. Analysis code and data sets data have been deposited in GitHub.com (https://github.com/DPGAVER/PNAS). Previously published data were used for this work (22).

ACKNOWLEDGMENTS. This work was funded by NIH R01HL142702, DoD W81XWH2010696, and NSF CBET 1706801 Grants.

Author affiliations: [a]Department of Biomedical Engineering, Tulane University, New Orleans, LA 70118; [b]Department of Surgery, State University of New York Upstate Medical University, Syracuse, NY 13210; [c]Department of Trauma Critical Care Medicine, R Adams Cowley Shock Trauma Center, University of Maryland Medical Center, Baltimore, MD 21201; and [d]Department of Medicine, University of Vermont, Burlington, VT 05405

1. G. Bellani *et al.*, Epidemiology, patterns of care, and mortality for patients with acute respiratory distress syndrome in intensive care units in 50 countries. *JAMA* **315**, 788–800 (2016).
2. B. T. Thompson, R. C. Chambers, K. D. Liu, Acute respiratory distress syndrome. *N. Engl. J. Med.* **377**, 562–572 (2017).
3. A. S. Slutsky, V. M. Ranieri, Ventilator-induced lung injury. *N. Engl. J. Med.* **369**, 2126–2136 (2013).
4. N. Acute Respiratory Distress Syndrome, *et al.*, Ventilation with lower tidal volumes as compared with traditional tidal volumes for acute lung injury and the acute respiratory distress syndrome. *N. Engl. J. Med.* **342**, 1301–1308 (2000).
5. J. Villar *et al.*, The ALIEN study: Incidence and outcome of acute respiratory distress syndrome in the era of lung protective ventilation. *Intens. Care Med.* **37**, 1932–1941 (2011).
6. L. Gattinoni *et al.*, Ventilator-related causes of lung injury: The mechanical power. *Intens. Care Med.* **42**, 1567–1575 (2016).
7. T. Tonetti *et al.*, Driving pressure and mechanical power: New targets for VILI prevention. *Ann. Transl. Med.* **5**, 286 (2017).
8. F. Vasques *et al.*, Is the mechanical power the final word on ventilator-induced lung injury?-we are not sure. *Ann. Transl. Med.* **6**, 395 (2018).
9. L. Gattinoni, F. Collino, L. Camporota, Mechanical power: Meaning, uses and limitations. *Intens. Care Med.* **49**, 465–467 (2023).
10. J. J. Marini, L. T. Thornton, P. R. M. Rocco, L. Gattinoni, P. S. Crooke, Practical assessment of risk of VILI from ventilating power: A conceptual model. *Crit Care* **27**, 157 (2023).
11. M. Busana *et al.*, Energy dissipation during expiration and ventilator-induced lung injury: An experimental animal study. *J. Appl. Physiol.* **1985**, 1212–1219 (2022).
12. J. H. T. Bates, D. W. Kaczka, M. Kollisch-Singule, G. F. Nieman, D. P. Gaver III, Mechanical Power and Ventilator-induced Lung Injury: What Does Physics Have to Say? *Am. J. Respir Crit. Care Med.* **209**, 787–788 (2024).
13. D. A. Kaminsky, What does airway resistance tell us about lung function? *Respir Care* **57**, 85–96; discussion 96–89 (2012).
14. J. A. Zasadzinski, J. Ding, H. E. Warriner, F. Bringezu, A. J. Waring, The physics and physiology of lung surfactants. *Curr. Opin. Colloid Interface Science* **6**, 506–513 (2001).
15. J. Mead, T. Takishima, D. Leith, Stress distribution in lungs: A model of pulmonary elasticity. *J. Appl. Physiol.* **28**, 596–608 (1970).
16. J. Mead, J. L. Whittenberger, J. E. P. Radford, Surface tension as a factor in pulmonary volume-pressure hysteresis. *J. Appl. Physiol.* **10**, 191–196 (1957).
17. D. P. Gaver III, D. Halpern, O. E. Jensen, "Surfactant and Airway Liquid Flows" in *Molecular Mechanisms in Lung Surfactant (Dys)function*, K. Nag, Ed. (Marcel Dekker, New York, 2005), pp. 187–223.
18. D. Huh *et al.*, Acoustically detectable cellular-level lung injury induced by fluid mechanical stresses in microfluidic airway systems. *Proc. Natl. Acad. Sci. U.S.A.* **104**, 18886–18891 (2007).
19. J. Rasanen, M. E. Nemergut, N. Gavriely, Changes in breath sound power spectra during experimental oleic acid-induced lung injury in pigs. *J. Appl. Physiol.* **1985**, 61–66 (2014).
20. J. Rasanen, M. E. Nemergut, N. Gavriely, Effect of PEEP on breath sound power spectra in experimental lung injury. *Intens. Care Med. Exp.* **2**, 25 (2014).
21. A. D. T. Force *et al.*, Acute respiratory distress syndrome: The Berlin Definition. *JAMA* **307**, 2526–2533 (2012).
22. H. Ramcharran *et al.*, Protective ventilation in a pig model of acute lung injury: Timing is as important as pressure. *J. Appl. Physiol.* **1985**, 1093–1105 (2022).
23. T. J. Pedley, R. C. Schroter, M. F. Sudlow, Energy losses and pressure drop in models of human airways. *Respir Physiol.* **9**, 371–386 (1970).
24. K. Von Neergaard, Neue auffassungen über einen grundbegriff der atemmechanik. Die retraktionskraft der lunge, abhängig von der oberflächenspannung in den alveolen. *Z. Gesamte Exp. Med.* **66**, 373–394 (1929).
25. J. C. Smith, D. Stamenovic, Surface forces in lungs. I. Alveolar surface tension-lung volume relationships. *J. Appl. Physiol.* **60**, 1341–1350 (1986).
26. G. M. Albaiceta, L. Blanch, Beyond volutrauma in ARDS: The critical role of lung tissue deformation. *Crit Care* **15**, 304 (2011).

27. A. M. Bilek, K. C. Dee, D. P. Gaver III, Mechanisms of surface-tension-induced epithelial cell damage in a model of pulmonary airway reopening. *J. Appl. Physiol.* **94**, 770–783 (2003).
28. S. S. Kay, A. M. Bilek, K. C. Dee, D. P. Gaver, Pressure gradient, not exposure duration, determines the extent of epithelial cell damage in a model of pulmonary airway reopening. *J. Appl. Physiol.* **97**, 269–276 (2004).
29. D. P. Gaver III, A. M. Jacob, A. M. Bilek, K. C. Dee, "The significance of air-liquid interfacial stresses on low-volume ventilator-induced lung injury" in *Ventilator-Induced Lung Injury*, D. Dreyfuss, G. Saumon, R. D. Hubmayr, Eds. (Taylor & Francis, New York, London, 2006), **vol. 215**, pp. 157–203.
30. C. Novak, M. N. Ballinger, S. Ghadiali, Mechanobiology of pulmonary diseases: A review of engineering tools to understand lung mechanotransduction. *J. Biomech. Eng.* **143**, 110801 (2021).
31. H. L. Dailey, L. M. Ricles, H. C. Yalcin, S. N. Ghadiali, Image-based finite element modeling of alveolar epithelial cell injury during airway reopening. *J. Appl. Physiol.* **106**, 221–232 (2009).
32. N. Higuita-Castro *et al.*, Using a novel microfabricated model of the alveolar-capillary barrier to investigate the effect of matrix structure on atelectrauma. *Sci. Rep.* **7**, 11623 (2017).
33. J. B. Grotberg, Crackles and wheezes: Agents of injury? *Ann Am Thorac Soc* **16**, 967–969 (2019).
34. D. P. Gaver III, R. W. Samsel, J. Solway, Effects of surface tension and viscosity on airway reopening. *J. Appl. Physiol.* **69**, 74–85 (1990).
35. D. P. Gaver, D. Halpern, O. E. Jensen, J. B. Grotberg, The steady motion of a semi-infinite bubble through a flexible-walled channel. *J. Fluid Mech.* **319**, 25–65 (1996).
36. E. Yamaguchi *et al.*, Electric cell-substrate impedance sensing (ECIS) as a Platform for evaluating barrier-function susceptibility and damage from pulmonary atelectrauma. *Biosensors (Basel)* **12**, 390 (2022).
37. E. Yamaguchi, L. P. Nolan, D. P. Gaver III, Microscale distribution and dynamic surface tension of pulmonary surfactant normalize the recruitment of asymmetric bifurcating airways. *J. Appl. Physiol.* **1985**, 1167–1178 (2017).
38. A. M. Jacob, D. P. Gaver III, Atelectrauma disrupts pulmonary epithelial barrier integrity and alters the distribution of tight junction proteins ZO-1 and claudin 4. *J. Appl. Physiol.* **1985**, 1377–1387 (2012).
39. S. N. Ghadiali, D. P. Gaver, Biomechanics of liquid-epithelium interactions in pulmonary airways. *Respir Physiol. Neurobiol* **163**, 232–243 (2008).
40. S. Ghadiali, Y. Huang, Role of airway recruitment and derecruitment in lung injury. *Crit Rev. Biomed. Eng.* **39**, 297–317 (2011).
41. M. Heil, Airway closure: Occluding liquid bridges in strongly buckled elastic tubes. *J. Biomech. Eng-T Asme* **121**, 487–493 (1999).
42. J. B. Grotberg, Respiratory fluid mechanics. *Phys. Fluids (1994)* **23**, 21301 (2011).
43. M. Muradoglu, F. Romanò, H. Fujioka, J. B. Grotberg, Effects of surfactant on propagation and rupture of a liquid plug in a tube. *J. Fluid Mech.* **872**, 407–437 (2019).
44. H. Fujioka, F. Romano, M. Muradoglu, J. B. Grotberg, Splitting of a three-dimensional liquid plug at an airway bifurcation. *Phys. Fluids (1994)* **34**, 081907 (2022).
45. J. W. Song, J. Paek, K. T. Park, J. Seo, D. Huh, A bioinspired microfluidic model of liquid plug-induced mechanical airway injury. *Biomicrofluidics* **12**, 042211 (2018).
46. D. P. Gaver III *et al.*, The POOR Get POORer: A hypothesis for the pathogenesis of ventilator-induced lung injury. *Am. J. Respir Crit. Care Med.* **202**, 1081–1087 (2020).
47. E. T. Naureckas *et al.*, Airway reopening pressure in isolated rat lungs. *J. Appl. Physiol.* **76**, 1372–1377 (1994).
48. B. Suki, A.-L. Barabasi, Z. Hantos, F. Petak, H. E. Stanley, Avalanches and power-law behaviour in lung inflation. *Nature* **368**, 615–618 (1994).
49. S. Reichert, R. Gass, C. Brandt, E. Andres, Analysis of respiratory sounds: State of the art. *Clin. Med. Circ Respirat Pulm Med.* **2**, 45–58 (2008).
50. B. Asgharian *et al.*, Modeling particle deposition in the pig respiratory tract. *J Aerosol Sci* **99**, 107–124 (2016).
51. L. Gattinoni, A. Pesenti, The concept of "baby lung". *Intens. Care Med.* **31**, 776–784 (2005).
52. D. R. Myers, *Solar Radiation: Practical Modeling for Renewable Energy Applications* (CRC Press, 2017).
53. H. Ma, H. Fujioka, D. Halpern, J. H. T. Bates, D. P. Gaver III, Full-lung simulations of mechanically ventilated lungs incorporating recruitment/derecruitment dynamics. *Front Netw Physiol.* **3**, 1257710 (2023).
54. K. E. Swenson, E. R. Swenson, Pathophysiology of acute respiratory distress syndrome and COVID-19 lung injury. *Crit. Care Clin.* **37**, 749–776 (2021).
55. C. O. Ciutara, S. V. Iasella, B. Huang, S. Barman, J. A. Zasadzinski, Evolution of interfacial mechanics of lung surfactant mimics progression of acute respiratory distress syndrome. *Proc. Natl. Acad. Sci. U.S.A.* **120**, e2309900120 (2023).
56. B. Gabela-Zuniga *et al.*, A micro-scale humanized ventilator-on-a-chip to examine the injurious effects of mechanical ventilation. *Lab Chip* **24**, 4390–4402 (2024).
57. I. Writing Group for the Alveolar Recruitment for Acute Respiratory Distress Syndrome Trial *et al.*, Effect of Lung recruitment and titrated positive end-expiratory pressure (PEEP) vs low PEEP on mortality in patients with acute respiratory distress syndrome: A randomized clinical trial. *JAMA* **318**, 1335–1345 (2017).
58. Y. Cui, R. Cao, Y. Wang, G. Li, Lung recruitment maneuvers for ARDS Patients: A systematic review and meta-analysis. *Respiration* **99**, 264–276 (2020).
59. A. M. Alencar, S. V. Buldyrev, A. Majumdar, H. E. Stanley, B. Suki, Avalanche dynamics of crackle sound in the lung. *Phys. Rev. Lett.* **87**, 088101 (2001).
60. J. A. Frank, M. A. Matthay, TGF-beta and lung fluid balance in ARDS. *Proc. Natl. Acad. Sci. U.S.A.* **111**, 885–886 (2014).
61. E. P. Judge *et al.*, Anatomy and bronchoscopy of the porcine lung. A model for translational respiratory medicine. *Am. J. Respir Cell Mol. Biol.* **51**, 334–343 (2014).
62. C. E. Bredenberg, A. M. Paskanik, G. F. Nieman, High surface tension pulmonary edema. *J. Surg. Res.* **34**, 515–523 (1983).
63. S. V. Jain *et al.*, The role of high airway pressure and dynamic strain on ventilator-induced lung injury in a heterogeneous acute lung injury model. *Intens. Care Med. Exp.* **5**, 25 (2017).
64. N. M. Habashi, Other approaches to open-lung ventilation: Airway pressure release ventilation. *Crit. Care Med.* **33**, S228–240 (2005).
65. J. H. T. Bates, D. W. Kaczka, M. Kollisch-Singule, G. F. Nieman, D. P. Gaver, Atelectrauma can be avoided if expiration is sufficiently brief: Evidence from inverse modeling and oscillometry during airway pressure release ventilation. *Crit. Care* **28**, 329 (2024).
66. J. H. T. Bates *et al.*, Altered airway mechanics in the context of obesity and asthma. *J. Appl. Physiol.* **1985**, 36–47 (2021).
67. J. R. Rodarte, K. Rehder, "Dynamics of respiration" in *Comprehensive Physiolology: Handbook of Physiology, The Respiratory System*, R. Terjung, Ed. (Wiley, Hoboken, NJ, 2011), pp. 131–144.
68. R. S. Harris, D. R. Hess, J. G. Venegas, An objective analysis of the pressure-volume curve in the acute respiratory distress syndrome. *Am. J. Respir Crit. Care Med.* **161**, 432–439 (2000).